Longitudinal electron beam and free electron laser microbunch measurements using off-phase rf acceleration

Kenneth N. Ricci* and Todd I. Smith

Stanford Picosecond FEL Center, W. W. Hansen Experimental Physics Laboratory, Stanford, California 94305-4085

(Received 2 February 2000; published 27 March 2000)

Magnetic dispersion followed by off-phase rf acceleration and an energy spectrometer were used to measure the longitudinal density profile of bunched relativistic electron beams with a resolution approaching 100 fs. Various electron bunch shapes were measured by this method and compared to bunch length measurements derived from the spectra of coherent transition radiation produced as the bunches traversed a thin foil. A reasonable agreement was found between the two bunch length methods. The off-phase rf acceleration method was then used to observe the modulated profile of a microbunched electron beam at the exit of a far-infrared free electron laser oscillator. In a preliminary study of the relationship between optical cavity power and the microbunch distribution, the density modulation and the energy spread of the electron beam were seen to increase as the optical field strength increased.

PACS numbers: 41.60.Cr, 29.27.–a

I. INTRODUCTION

In recent years the operation of many free electron lasers (FELs) and other accelerator-based light source experiments has required the production of increasingly short picosecond and subpicosecond relativistic electron bunches and the concurrent development of subpicosecond electron beam diagnostics. This paper describes applications of a novel subpicosecond beam diagnostic using magnetic longitudinal dispersion, an off-phase rf accelerator section, and an energy spectrometer.

Subpicosecond electron beam diagnostics range in complexity from very simple, such as an inexpensive thermal detector, to very elaborate optical/electronic instruments, such as the most advanced streak cameras. Since short picosecond electron bunches radiate more coherent millimeter- and submillimeter-wave electromagnetic radiation than longer bunches, the relative electron bunch length can be minimized in an accelerator simply by adjusting the beam injection parameters while monitoring the power of the coherent synchrotron radiation (CSR), coherent transition radiation (CTR), or other coherent radiation emitted by the beam at these frequencies [1–6]. Other diagnostics have attempted to measure the absolute bunch length and exact bunch shape, or longitudinal density profile. Techniques currently used for this purpose include streak cameras, optical gating, and spectral analysis of coherent radiation (CSR, CTR, etc.). All of these methods have succeeded in measuring subpicosecond bunch lengths, but they are limited in their ability to observe the bunch shape. Optical gating techniques require either extraordinarily good laser synchronization [7] or ambiguous pulse reconstruction [8], and they are complicated by the formation length and diffraction of the low-frequency components of the coherent fields [9]. Spectral techniques avoid the synchronization difficulty by working in the frequency domain instead of the time domain, but they suffer similar losses of low-frequency fields. Furthermore, only certain classes of bunch shapes can be reconstructed unambiguously from their power spectra [10]. A conventional streak camera attains high resolution in the time domain by using a ramped transverse electric field to transform a longitudinal (temporal) distribution of electrons into a more easily measured transverse distribution. With specialized optics designed by numerical simulation, resolutions of 200 fs have recently been reported [11].

A longitudinal variation of the streak camera principle has been used in multisection linear rf accelerators [12]. The last rf section is run off-phase so that the accelerating field is ramping up or down rapidly while a relativistic electron bunch passes through. Electrons entering the off-phase accelerator section receive an energy increment that varies in proportion to their time of arrival. This transforms the beam's temporal distribution into an energy distribution which can be observed in an energy spectrometer. In practice, the initial energy spread of the beam ΔE_{beam} limits the time resolution of this technique to $\Delta t = \Delta E_{\mathrm{beam}}/\alpha$, where α is the maximum available acceleration ramp (e.g., in keV/ps).

However, with an additional beam transformation from a longitudinally dispersive magnet section such as a chicane, the effect of initial beam energy spread can be removed from the final measurement. This idea was proposed by Crosson [13], and is illustrated in Fig. 1. In first-order

*Corresponding author. Telephone: (650)723-0209. FAX: (650)725-8311. Email address: kenricci@alum.mit.edu

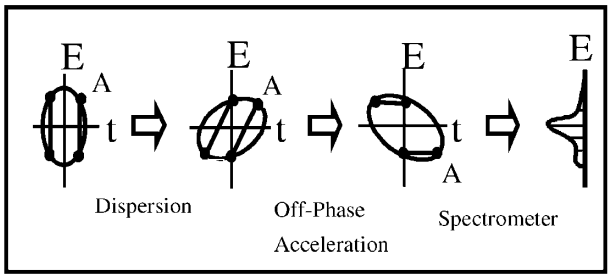

FIG. 1. A linear transformation of the longitudinal phase space can transform a temporal slice of the bunch, such as the segment containing point A, into a slice of the final energy distribution imaged in the spectrometer. Stretching of the phase space in the dispersive section allows an off-phase accelerator to remove the initial energy spread from the slice.

transport matrices, the chicane and off-phase acceleration transform the longitudinal beam phase space as

$$\begin{bmatrix} 1 & 0 \\ \alpha & 1 \end{bmatrix} \begin{bmatrix} 1 & \delta \\ 0 & 1 \end{bmatrix} \begin{bmatrix} t \\ E \end{bmatrix} = \begin{bmatrix} t + \delta E \\ \alpha t + (1 + \alpha\delta)E \end{bmatrix}, \quad (1)$$

where E is the energy coordinate relative to the mean energy of the bunch, t is the relative time or longitudinal position, and δ is the longitudinal dispersion of the chicane (e.g., in ps/keV). Notice that if the accelerator and chicane are adjusted so that $\alpha\delta = -1$, then the final energy coordinate will be $E_{\text{final}} = \alpha t_{\text{init}}$, with no first-order contribution from the initial energy distribution. This improvement to the off-phase rf acceleration technique yields a resolution of

$$\Delta t = \Delta E_{\text{spec}}/\alpha\,, \quad (2)$$

where the resolution ΔE_{spec} of the energy spectrometer is typically one or two orders of magnitude better than ΔE_{beam}. This has extended the resolution of the off-phase acceleration technique down to the femtosecond range and enabled a direct observation of the longitudinal profile of subpicosecond electron bunches [14]. At this resolution, it has become possible, for the first time, to observe the detailed temporal profile of an electron beam microbunched by the FEL interaction.

II. A COMPARISON OF TWO BUNCH MEASUREMENT TECHNIQUES

The new off-phase acceleration technique produced excellent longitudinal beam data that were compared with the results of a standard CTR spectral technique [15] in order to evaluate the effectiveness of the CTR method. Measurements were made using the part of the Stanford superconducting accelerator (SCA) shown schematically in Fig. 2. Bunches of 4×10^7 electrons were accelerated to 21 MeV and bunched to picosecond length by the SCA front end. The phase of the rf buncher and structures of the SCA front end were adjusted to vary the length and shape of the electron bunches, and for each setting the

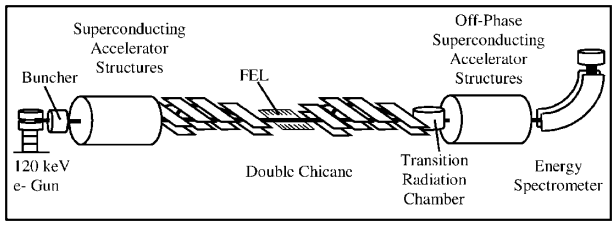

FIG. 2. Schematic diagram of part of the Stanford superconducting accelerator

bunch was alternately measured by off-phase acceleration and by CTR.

For the off-phase acceleration measurement, the beam passed through the chicanes and off-phase accelerator and was scanned across a thin tungsten wire at the focus of the energy spectrometer. The 1.3 GHz rf accelerator was run 90° off phase to provide an acceleration ramp $\alpha = 105$ keV/ps, and the chicanes were adjusted to provide the longitudinal dispersion $\delta = -0.0095$ ps/keV. The chicane dispersion was calculated from the chicane geometry and magnetic field and then optimized to within a few percent by tuning the chicane field until any energy increment added at the SCA front end was exactly canceled by the off-phase acceleration. This signaled the achievement of the condition $\alpha\delta = -1$ in the linear transport matrices. For the estimated 5π mm mrad normalized transverse emittances of this beam, the energy spectrometer had an observed resolution of 0.05%. According to Eq. (2), this corresponds to a time resolution of $0.05\% \times 21\ \text{MeV}/105\ \text{keV}\,\text{ps}^{-1} = 100$ fs.

For the CTR measurement, the chicanes were turned off, allowing the beam to travel in a straight line from the SCA front end to the CTR apparatus, shown schematically in Fig. 3. There the beam passed at a 45° incident angle through a thin, polished aluminum foil, producing forward and reflected transition radiation. The reflected CTR was collimated by a 50 mm diameter, 150 mm effective focal length parabolic reflector and analyzed in vacuum by a step-scanning Michelson interferometer to determine its spectrum by the Fourier transform method. The Michelson interferometer used a 3 mm thick TPX plastic beam splitter and a second parabolic reflector to focus the output light into a liquid helium cooled QMC Instruments[1] InSb bolometer.

The results of these dual measurements are shown in Fig. 4 for three different settings of the SCA front end. Figure 4(a) shows the three bunch shapes measured directly by the new off-phase acceleration technique. For

[1]Fast InSb detector type QFI/XB by QMC Instruments, West Sussex, England, mounted in dewar type HD-3 with a polyethylene window by Infrared Laboratories, Tucson, Arizona, 1993.

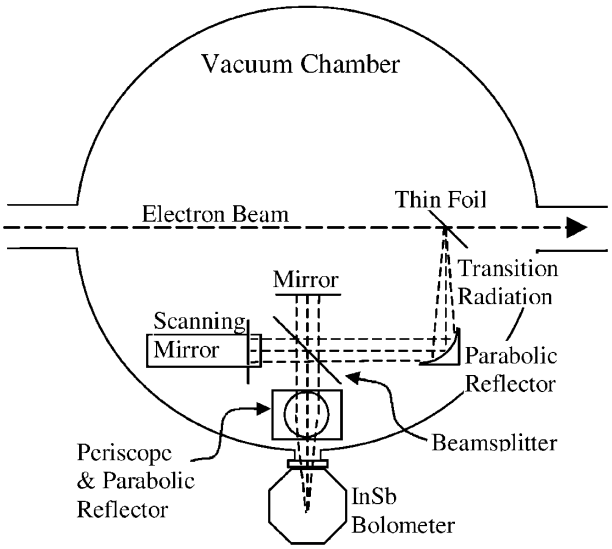

FIG. 3. Schematic diagram of the coherent transition radiation (CTR) measurement apparatus. As the beam passed at 45° incidence through a thin, polished aluminum foil, CTR was reflected from the foil into a parabolic mirror, which collimated the CTR and sent it through a Michelson interferometer.

clarity, bunch B1 has been shifted 2 ps to the left on the graph. The jaggedness of B2 and B3 is due to rf noise on the spectrometer wire and an intermittent 100 fs phase jitter between the beam and the rf accelerator during spectrometer scans. In order to verify the sharpness of its peak, bunch B1 was measured three times and averaged, removing much of the noise. The measured CTR spectra for the same three bunches are shown in Fig. 4(c). Since frequencies near zero could not be detected, the CTR spectra have been normalized to a value of 0.5 near the frequency 4.5 wave numbers for comparison with each other and with the power spectra of B1, B2, and B3, which were computed numerically by taking the square modulus of the Fourier transform of the profiles in 4(a). Figure 4(b) shows the shapes of the three bunches calculated from the measured CTR spectra using the extrapolation and Kramers-Kronig algorithm described in Ref. [15].

As expected, the shorter electron bunches emitted broader CTR power spectra in the millimeter and submillimeter wavelength range. Unfortunately, the measured CTR spectra do not agree well with the calculated spectra. At low frequencies this is easy to understand—a Fresnel calculation using the vectorial Smythe-Kirchoff approximation [16] for wave propagation through two 50 mm apertures separated by the 500 mm effective path length of the Michelson interferometer indicates that diffraction becomes severe for frequencies lower than four wave numbers. Measurements of the high frequency tails of the spectra were noisy because a background of charged particle and gamma-ray noise, particularly during the observation of bunches 1 and 3, limited the effective dynamic range of the bolometer to about 15 dB. Measurement of the higher frequencies was additionally

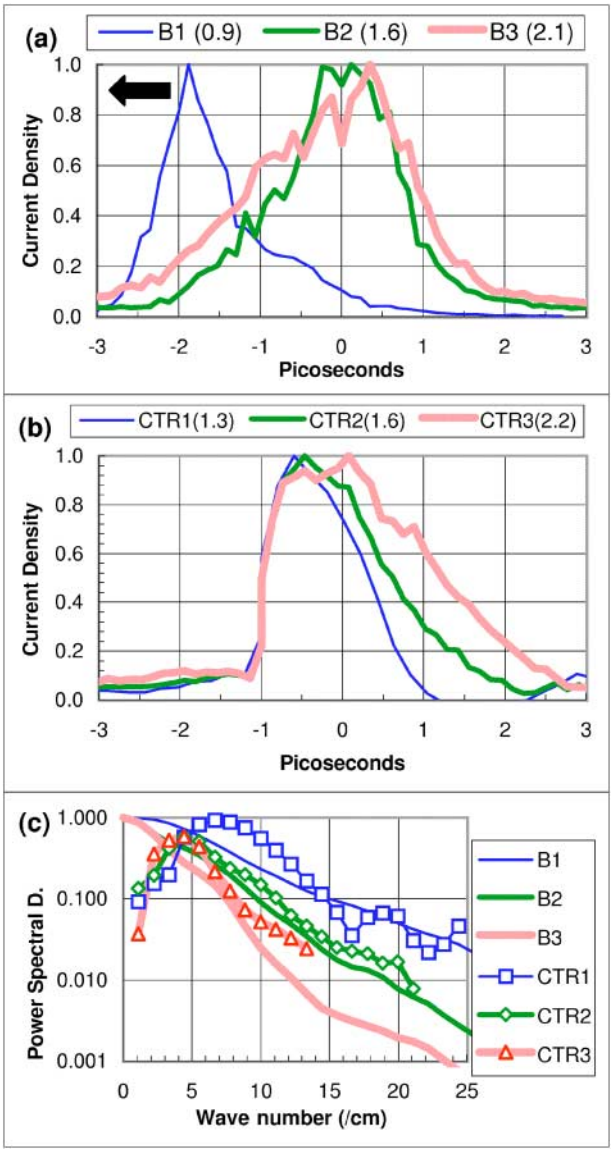

FIG. 4. (Color) Comparison of off-phase acceleration and CTR bunch shape measurements. (a) At three different accelerator settings, bunch shapes B1, B2, and B3 were observed by the new off-phase acceleration method. The peak heights have been normalized for ease in identifying their full width at half maximum (FWHM), given in parentheses (in picoseconds) for each bunch. The black arrow in the upper left indicates the direction of bunch travel (leading edge). (b) The shapes of the same three bunches were reconstructed by a CTR spectral method, which recovered the correct length and degree of asymmetry for bunches B2 and B3, but could not distinguish between the original bunch shape and its temporal reflection. The spectral method also failed to discover the sharpness of the peak and the shallow tail of bunch B1. (c) On a log scale, the normalized numerical power spectra of measured bunch shapes B1–B3 are compared with the measured CTR spectral data CTR1–CTR3 to show how detector response may affect bunch shape retrieval.

hampered by the nonlinearity of the InSb bolometer's spectral response. Using a mercury vapor lamp in a Bruker Fourier transform infrared (FTIR) spectrometer,

and the SUNSHINE [17] coherent terahertz light source with a Michelson interferometer similar to the one in Fig. 3, the spectral response of the InSb detector was estimated over the range from 5 to 50 wave numbers; it was found to be approximately one order of magnitude less sensitive at 30 wave numbers than at 10 wave numbers. This nonlinearity further reduced the effective dynamic range of the detector for this application. A Molectron P1-75cc pyroelectric detector was substituted in place of the InSb bolometer and was found to have even greater nonlinearity over this spectral range.

When applied to imperfect spectral data like this, the Kramers-Kronig algorithm produces an artifact in its bunch shape reconstruction. Every bunch has the same extremely sharp rising edge, a result which is clearly not physical. Furthermore, like any method based solely on a power spectrum, the Kramers-Kronig algorithm cannot distinguish between any particular asymmetric pulse and its temporal reflection, which has an identical power spectrum. In spite of detection and algorithm shortcomings, there was sufficient optical information to calculate the absolute electron bunch length and the degree of asymmetry for the relatively simple shapes of B2 and B3. The sharp peak and shallow tail of B1 produce more CTR at the high and low frequency extremes, where the optical detection is poor, and so it is not surprising that these features are not well reconstructed. The reconstruction CTR1 overestimates the FWHM of B1 by about 40%, but underestimates the temporal standard deviation σ_t by 20%—σ_t for the reconstruction CTR1 is 0.57 ps, while the actual deviation σ_t is 0.71 ps for B1.

For smooth Gaussian bunches, the FWHM is always $2.35 \times \sigma_t$, making these two statistical definitions of bunch length equivalent. Clearly, the notion of *absolute bunch length,* a single statistical parameter describing the duration of the bunch, does not apply as well to irregular distributions like B1. However, if the definition of bunch length is taken to be the average of $2.35 \times \sigma_t$ and the bunch FWHM, then the off-phase acceleration and CTR methods yielded the same average bunch length in all three cases to within a few percent. This comparison showed that, with imperfect optical data, CTR and other spectral methods can correctly measure the electron bunch length, but they miss significant details of the bunch shape, which can be observed by a direct method such as the new off-phase acceleration technique.

III. RESOLUTION LIMITS

During the measurements in Sec. II of this paper, the sharpest bunch feature consistently resolved (the averaged tip of bunch B1) had a width of 130 ± 10 fs. The resolution was limited mainly by the maximum available acceleration ramp α and the spectrometer resolution ΔE. It is reasonable to assume that with a greater acceleration ramp or a smaller focus in the spectrometer, this resolution would improve significantly. However, at resolutions below 100 fs, care must be taken to consider second-order terms in longitudinal beam transport and coupling between the transverse and longitudinal phase spaces of the beam. Following the notation of Refs. [18,19], these terms will be described using the linear transport coefficients R_{ij} and second-order coefficients T_{ijk}, where the subscripts i, j, k range over the six-dimensional phase-space coordinates $(x, \dot{x}, y, \dot{y}, t, E)$ of the beam. For example, the second-order contribution from the dimensionless $\dot{y}$ momentum to the longitudinal position t after a drift section of length L is written as

$$\Delta t = \frac{L}{2c}(\dot{y})^2 \equiv T_{544}(\dot{y})^2.$$

Table I indicates the estimated size of all first- and second-order longitudinal terms for the measurement described in Sec. II of this paper. For brevity, the relevant components of Fig. 2 have been entered into the table in five lumped sections: (i) the chicane section, whose primary purpose is to provide the linear longitudinal dispersion $R_{56} \equiv \delta$ as indicated in the table; (ii) a short drift section with quadrupoles to transport the beam from the chicanes to the final accelerator section; (iii) the off-phase accelerator; (iv) another short drift section with quadrupoles to match the beam into the spectrometer; and (v) the energy spectrometer. Several entries in the table merit particular attention. The temporal terms R_{5j} and T_{5jk} after the off-phase accelerator are unimportant for this type of measurement because the distribution of interest after that point is the energy distribution. The largest second-order terms in the table are the quadrupole focusing terms $T_{511}, T_{512}, T_{533}, \ldots$ over a 6 m drift section after the chicanes, estimated at 60 fs each for the $x, \dot{x}$ and $y, \dot{y}$ phase spaces. Assuming a Gaussian electron distribution in all phase-space coordinates, the best expected resolution including first- and second-order terms would be about 140 fs, in good agreement with observations.

Since the focusing terms increase quadratically with transverse emittance, significant improvement may be expected with a better beam quality. Typical transverse emittances in the SCA are $5-10\pi$ mm mrad, but the newest generation of linear accelerators can achieve transverse emittances on the order of 1π mm mrad, making the focusing terms negligible. Unfortunately, the situation is not so hopeful for the nonlinear longitudinal dispersion term T_{566} of the chicane. Some energy spread is needed to produce a picosecond bunched beam, and this energy spread will cause a nonlinear smearing of the longitudinal structure at the femtosecond level as the beam passes through a chicane. So, in higher gradient accelerators with lower emittances, the 140 fs resolution of this off-phase rf acceleration method could be improved to the 20–30 fs level, where the limiting term will be the T_{566} of the chicane.

TABLE I. Beam phase-space coupling coefficients for the beam transport used in longitudinal bunch profile measurements. Symbols used are L: effective path length of a beam transport section; f: effective focal length of a magnetic lens or dipole fringe field; b: spacing between chicane dipoles; r, θ: bend radius and bend angle in chicane dipoles; $v = \beta c$: electron drift velocity; τ, ψ: rf period and phase of the off-phase accelerator.

	First order R_{ij}	Second order T_{ijk}
Chicane	$R_{55} = 1$	$T_{51j} = 0$
	$R_{56} \equiv \delta = -95$ fs/keV	$T_{522} \Rightarrow \frac{L}{2c}\dot{x}^2 \lesssim 20$ fs
	$R_{65} = 1$	$T_{533}, T_{534}, T_{544} \Rightarrow \frac{L}{2c}(\dot{y}^2 + \frac{y}{f})^2 \lesssim 20$ fs
	all other $R_{5j}, R_{6j} = 0$	$T_{566} = \frac{1}{2}\frac{\partial^2 L}{\partial E^2} \Rightarrow (4r\tan^3\theta + \frac{6b\tan^2\theta}{\cos^3\theta})\frac{(\Delta E)^2}{2cE^2} \lesssim 30$ fs
		all other $T_{5jk} = 0$
		$T_{6jk} = 0$
Quadrupoles and first drift section	$R_{55} = 1$	$T_{511}, T_{512}, T_{522} \Rightarrow \frac{L}{2c}[\dot{x}^2 + (\frac{x}{f})^2] \lesssim 60$ fs
	$R_{56} = -\frac{\partial v}{\partial E} \ll \delta_{\text{chicane}}$	$T_{533}, T_{534}, T_{544} \Rightarrow \frac{L}{2c}[(\dot{y})^2 + (\frac{y}{f})^2] \lesssim 60$ fs
	$R_{66} = 1$	$T_{566} \Rightarrow \frac{\partial^2 v}{\partial E^2}\frac{L(\Delta E)^2}{2c^2} \lesssim 5$ fs
	all other $R_{5j}, R_{6j} = 0$	all other $T_{5jk}, T_{6jk} = 0$
Off-phase accelerator	$R_{55} = 1$	$T_{655} \Rightarrow \Delta E \propto \frac{2\pi^2 t^2 \cos(\psi)}{\tau^2}$
	$R_{65} = \alpha = 105$ keV/ps	
	$R_{66} = 1$	
	all other $R_{5j}, R_{6j} = 0$	
Second drift section	R_{5j} unimportant	T_{5jk} unimportant
	$R_{6j} = 0$	$T_{6jk} = 0$
Spectrometer	$\frac{\Delta E_{\text{spec}}}{\alpha} = 100$ fs	T_{5jk} unimportant
		$T_{6jk} = 0$

IV. DIRECT OBSERVATION OF FEL MICROBUNCHES

It is well known that undulator and optical fields interact with an electron beam in a free electron laser to modulate the electron beam energy and density periodically at the optical wavelength of the laser, forming microbunches that coherently excite the optical field [20]. The increasing optical field in turn increases the rate of microbunching, providing the positive feedback mechanism for FEL gain, until the field-induced energy spread or energy loss of the beam causes enough of the current to slip out of resonance with the optical bandwidth that the net gain drops to zero and the FEL saturates. For the case where large energy spread causes saturation, the beam may overbunch—the optical field induces such a large spread in electron drift velocities that microbunches form and then disperse again before completing a pass through the undulator. In a short-pulse FEL oscillator where the electron bunch, optical pulse, and slippage distance are close to the same length, the electron bunch coherence at saturation will vary as a function of optical power, slippage length, and the desynchronism between the optical pulse and electron bunch periods [21]. While the occurrence of gain in an FEL confirms the existence of microbunching, it has not been possible until now to observe the density modulation directly, because the interval between optical periods was too short. Instead, indirect measurements of modulation depth have been made by observing the power spectrum of coherent transition radiation emitted from a beam microbunched in a mid-infrared SASE FEL [22]. Now, however, the complete longitudinal profiles of beams microbunched by the FIREFLY free electron laser have been imaged using the dispersion-improved off-phase rf acceleration technique at the Stanford Picosecond FEL Center.

TABLE II. Typical FIREFLY parameters for 60 μm microbunch observations.

Undulator period	$\lambda_u = 6$ cm
Number of periods	$N_u = 25$
Undulator (K)	$K_u = 1.0$
Bunch charge	$1.3 \times 10^8 e^-$
Electron bunch length	1.7 ps FWHM
Beam energy	16 MeV
Initial beam energy spread	130 keV FWHM
Beam repetition rate	11.8 MHz
Optical wavelength	60 μm
Slippage length	1.5 mm
Optical cavity length	12.7 m
Maximum optical gain	1.3% per pass
Cavity (Q)	30
Intracavity optical power[a]	~40 W

[a]Estimated cw average optical power extracted from the 11.8 MHz pulsed electron beam at FEL saturation.

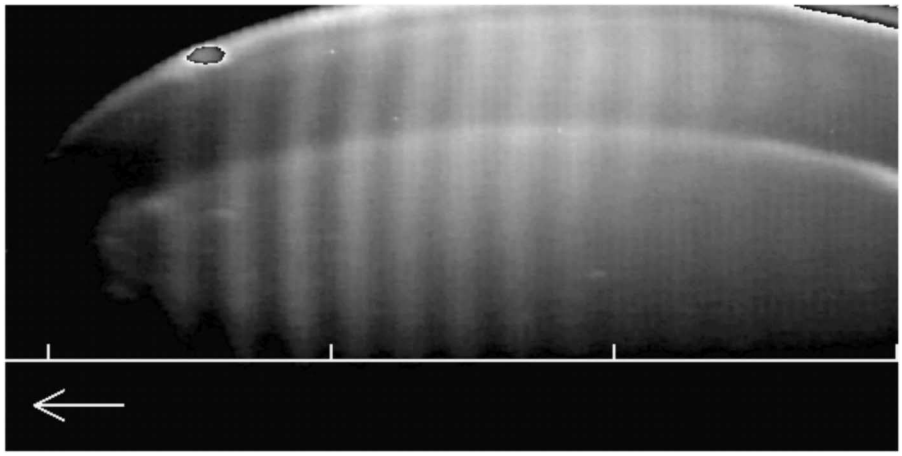

FIG. 5. A gray-scale image of 60 μm FIREFLY microbunches focused in the energy spectrometer. The energy distribution of the final beam, dispersed horizontally in this image, exhibits the time profile of the beam at the undulator exit. The light colored vertical bars are regions of higher electron density (microbunches). The two horizontal white arcs are optical artifacts (reflections from the edge of the scintillator). The scale and arrow at the bottom of the image indicate picoseconds and the direction of bunch travel.

For these measurements, the energy spectrometer instrumentation was upgraded from a slow-scanning tungsten wire to a scintillator screen and camera which can acquire an energy spectrum in 30 μs. This eliminated rf electrical noise and the rf/beam phase jitter on millisecond and longer time scales. FIREFLY was operated at wavelengths between 51 and 60 μm, as measured with an ARC[2] far-infrared diffraction grating monochromator. For other FIREFLY parameters, see Table II. The electron beam was coupled into and out of the FIREFLY optical cavity using the electromagnetic chicanes illustrated in Fig. 2. The second chicane, at the output end of the FIREFLY undulator, was adjusted to provide -0.018 ps/keV longitudinal dispersion. A beam of 1.3×10^8 electrons per bunch excited the FIREFLY laser and was microbunched in the undulator. At the exit of the undulator, apertures reduced the current to about 5×10^7 electrons per bunch to trim the transverse emittance and permit a better resolution at the spectrometer. After the beam received an off-phase acceleration of 56 keV/ps, its energy distribution was imaged on a YAG:Ce scintillator screen at the focus of the spectrometer. A monochrome charge-coupled device (CCD) camera[3] with a triggered 30 μs electronic shutter was used to select and integrate a train of 350 bunches from the 11.8 MHz pulsed electron beam. In principle, with a fast gated intensified camera, it would be possible to observe the longitudinal profile of a single bunch this way.

A typical image of 60 μm FIREFLY microbunches is shown in Fig. 5. The strongest beam modulation usually occurred at the peak of the electron bunch, but in some cases, such as the 60 μm modulated profile shown in Fig. 6, the microbunches were distributed asymmetrically with the maximum modulation shifted toward either the leading or trailing edge. No strong correlation has yet been found between the occasional microbunching asymmetry and any controlled FEL parameter. When the FIREFLY wavelength was changed from approximately 60 to 51 μm by adjusting the electromagnetic undulator strength without adjusting beam energy or other parameters, the spacing of the microbunches shortened accordingly, as shown in Fig. 6.

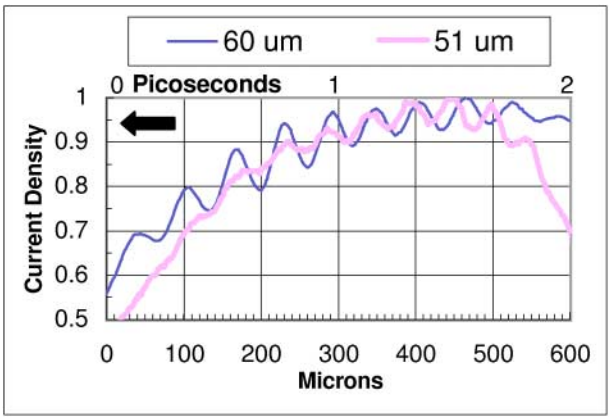

FIG. 6. (Color) Normalized beam current density with microbunching at 60 and 51 μm. These data were averaged from 60 horizontal slices through images like Fig. 5. Note that the modulation amplitude varies along the electron bunch. The arrow indicates the direction of bunch travel.

[2]SpectroPro VM-504 Monochromator by Acton Research Corporation, Massachusetts, 1993.

[3]Pulnix TM-7AS CCD camera from Pulnix America Inc., Sunnyvale CA 1999

V. ANALYSIS OF MICROBUNCH OBSERVATIONS

Microbunches at 60 μm spacing were observed for a variety of FEL parameters and found to be extremely sensitive to changes in the optical cavity desynchronism, as indicated by Fig. 7(a). Here, *desynchronism* is defined as the repetition period of the electron beam minus the round-trip time of the optical cavity, so that desynchronism increases as the cavity length decreases. It is difficult to determine the absolute desynchronism while the FEL is operating, but the relative desynchronism can be precisely adjusted by changing the optical cavity length. (Note that the round-trip optical path length changes by twice as much as the cavity length changes.)

At relatively small desynchronism, where the saturated optical field was strongest (relative cavity length 0 to -1 μm), and at large desynchronism, where the saturated optical field was weak (relative cavity length -7 to -10 μm), no microbunches were observed, but beam modulation up to 12% was measured for intermediate values of the desynchronism. These data imply that the microbunches at large desynchronism were too small to see above background noise and that the microbunch measurement at small desynchronism was disrupted by FEL-induced energy spread. The disappearance of microbunches at strong optical fields also suggests the possibility of overbunching, but careful consideration of the beam energy spread shown in Fig. 7(b) rules out this conjecture.

Two electrons with a small energy difference ΔE move at slightly different velocities,

$$\frac{\Delta v}{v} \approx \frac{1}{\gamma^2}\frac{\Delta E}{E}, \tag{3}$$

with relativistic factor γ. After they traverse an undulator trajectory of length $N_u\lambda_u(1 + K^2)$, their longitudinal phase shift with respect to each other is

$$\Delta\phi = 4\pi N_u \frac{\Delta E}{E}, \tag{4}$$

where $\Delta\phi$ is given in radians of the optical wavelength

$$\lambda_0 \approx \frac{\lambda_u(1 + K^2)}{2\gamma^2}. \tag{5}$$

Here N_u, λ_u, and K are the number of periods, period length, and dimensionless field strength [20] of the undulator. In the case of field-induced energy spread, the electrons do not move uniformly with respect to each other but are accelerated as a function of their phase relative to the optical wave. In the limit of a continuous-wave (cw), weak optical field, the acceleration a is nearly uniform on an electron at resonance with the undulator field, so that the velocity varies linearly as $\Delta v = aT$ and the phase shift varies as $\Delta\phi \propto \frac{1}{2}aT^2 = \frac{1}{2}vT$, where T is the time elapsed during transit. Then the phase shift at the undulator exit due to a uniform acceleration is related to the final induced energy spread by

$$\Delta\phi = 2\pi N_u \frac{\Delta E_{\text{ind}}}{E}. \tag{6}$$

When optimal bunching occurs, the maximal phase shift of some of the electrons must reach $\pm\pi$ radians [20].

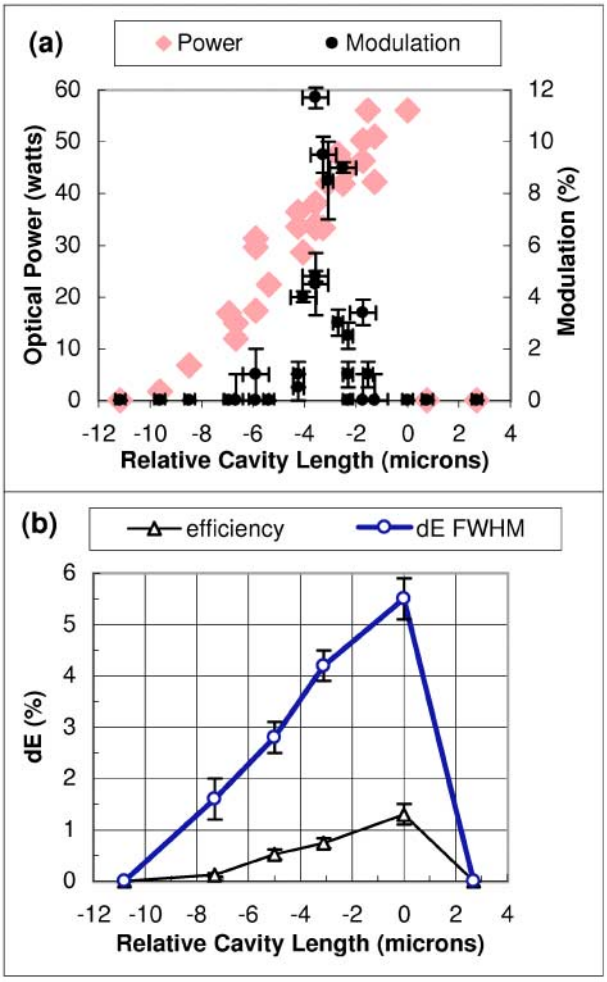

FIG. 7. (Color) (a) Measured microbunch modulation amplitude and FEL power as a function of optical cavity length. Since the absolute cavity desynchronism was difficult to determine during FEL operation, the relative cavity length was defined as zero at the smallest desynchronism (longest cavity length) where stable lasing occurred. Modulation percent is defined as one-half of the maximum peak-to-peak variation in electron beam density divided by the mean density over one wavelength. Power indicates the cw average of the intracavity optical power extracted from the 11.8 MHz pulsed electron beam. The relative FEL power was monitored with a far-infrared detector, and an absolute calibration was estimated from the observed efficiency (defined below). (b) FEL-induced beam energy spread and efficiency as a function of optical cavity length. Efficiency is defined as the FEL-induced change in the mean electron energy divided by the initial mean electron energy.

Plugging this into Eq. (6) and solving for the expected energy spread, we find

$$\frac{\Delta E_{\text{ind}}}{E} \approx \pm\frac{1}{2N_u} \tag{7}$$

for optimal bunching. This expression must be taken only as a conservative lower limit on the energy spread required to achieve optimal bunching because electron acceleration in a strong optical field is not uniform and, particularly, because of the unique properties of short-pulse FEL oscillators.

It is generally known that at large desynchronism the optical field in a short-pulse FEL oscillator is strongly asymmetric [21], and the peak of the optical pulse interacts with the electron bunch only at the end of the undulator. In this situation, much of the energy spread (first integral of acceleration) is imparted to the beam too late to microbunch the beam (second integral of acceleration) effectively. At small desynchronism, the optical pulse tends to be nearly symmetric and significantly shorter than the slippage length due to the effect known as lethargy [21], so that the effective FEL interaction length is reduced. This increases the optical bandwidth and also requires a larger field-induced energy spread to achieve optimal bunching in the shorter effective undulator length.

The FEL-induced electron energy spread and FEL efficiency were determined by comparing the beam energy distributions with and without FIREFLY lasing, as shown in Fig. 8. For the 25-period undulator of FIREFLY, Eq. (7) predicts that strong bunching should not appear until the induced energy spread approaches $\pm 2\%$, or 4% FWHM, in good agreement with Figs. 7(a) and 7(b). For relative cavity lengths less than -6 μm, the optical field saturated at low intensity because the large desynchronism decreased the coupling of the electron beam with the peak of the optical pulse, lowering the optical gain. A small field-induced energy spread was enough to decrease the gain to zero and cause saturation. At relative cavity lengths near -4 μm, the desynchronism was nearly optimal for coupling of the electron beam to the optical pulse, and the highest optical gain (1.3% per pass) was observed. Higher initial gain enabled the FEL interaction to proceed to larger energy spreads and stronger microbunching before reaching saturation. Smaller desynchronism also produced a shorter optical wave train with a broader gain spectrum. At relative cavity length 0, FIREFLY had an optical bandwidth of 3.5% as measured with the ARC monochromator. This bandwidth corresponds to a wave train 14 periods long, indicating that the optical pulse had shortened enough to reduce the effective FEL interaction length by 45%. Recalling Eq. (7), the energy spread needed to fully bunch the beam in a 14-period undulator is at least

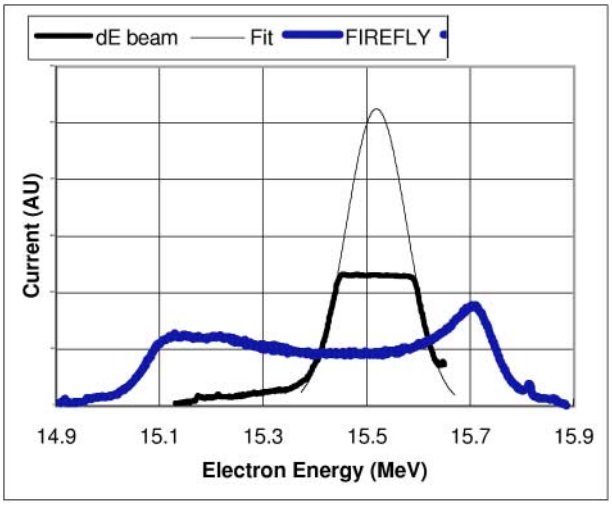

FIG. 8. (Color) Typical measured beam energy spreads with and without FIREFLY lasing. The unperturbed beam had an energy spread of about 130 keV FWHM as shown by the equal-area fit. (The spectrometer camera was saturated for this measurement.) With FIREFLY lasing at this particular desynchronism, the induced energy spread was 4.4% and the FEL efficiency (mean energy loss of the beam) was 0.7%.

$$\frac{\Delta E}{E} \approx \pm\frac{1}{2N_{\text{eff}}} = \pm 3.5\%\,, \tag{8}$$

or 7% FWHM. The 5.5% energy spread measured at this desynchronism was still insufficient to produce overbunching.

However, the increased energy spread had an adverse effect on the measurement, because femtosecond longitudinal resolution can be achieved only when the second-order beam transport terms are small. For the measurements shown in Fig. 7, the T_{566} coupling from beam energy to longitudinal position in the chicane became significant as the energy spread exceeded 4% FWHM. With chicane parameters $r = 42$ cm, $\theta = 0.39$, $b = 13$ cm (from Table I), the T_{566} temporal distortion was

$$\left(4r\tan^3\theta + \frac{6b\tan^2\theta}{\cos^3\theta}\right)\frac{(\Delta E)^2}{2cE^2} = 190\text{ fs} \quad \text{when } \frac{\Delta E}{E} = \pm 0.02\,, \tag{9}$$

which smeared out the 200 fs separation between 60 μm microbunches. Since this distortion increased quadratically with energy spread, it cut off the observable microbunches sharply as the relative cavity length was increased from -4 to -2 μm. As the cavity length approaches zero and the optical field continues to increase, the microbunching is also expected to increase, but this cannot be observed using the phase-acceleration method unless steps are taken to trim the induced energy spread after the undulator and before the off-phase accelerator.

VI. CONCLUSIONS

The longitudinal beam dispersion of a magnetic chicane and an off-phase linear accelerator section have been used with an energy spectrometer to measure the longitudinal density profile of relativistic electron bunches at the Stanford superconducting accelerator with a resolution approaching 100 fs. This diagnostic was used to observe a variety of bunch shapes produced by beam manipulation at the accelerator front end and was compared with another standard subpicosecond bunch measurement technique: the spectral analysis of CTR. The new off-phase acceleration technique yielded similar results for overall bunch length measurement, but offered a direct view of the bunch shape that was far superior to the bunch shape information inferred from CTR.

The accuracy and effectiveness of the new off-phase acceleration technique were further demonstrated by making the first direct time-domain observation of the profile of an FEL microbunched electron beam. Trains up to 13 microbunches long were resolved at separations of 51 and 60 μm, conclusively showing a resolution better than 170 fs and temporal linearity of the technique over a range of several picoseconds. In the first experimental study of microbunching as a function of desynchronism in an FEL oscillator, the saturated optical power, beam energy spread, and beam modulation amplitude increased as desynchronism decreased, at rates which indicated a gain-bandwidth limited saturation process instead of longitudinal overbunching of the beam.

In higher gradient accelerators with smaller emittances, this improved off-phase acceleration measurement technique could be extended to resolutions of tens of femtoseconds, with the ultimate resolution limited by second-order terms in the beam transport such as the nonlinear longitudinal dispersion (T_{566}) of a magnetic chicane. This femtosecond beam diagnostic may be useful in accelerator facilities that require well-characterized ultrashort electron bunches for coherent terahertz light generation, fast IR/UV/x-ray light sources, or high current density applications such as FEL, SASE FEL, and high brightness beams.

ACKNOWLEDGMENTS

The authors wish to thank Eric R. Crosson for his role in extending the wavelength capability of FIREFLY for this experiment and Takuji Kimura for assistance in making microbunch measurements. Funding was provided in part by ONR Grant No. N000140-94-1-1024.

[1] D. X. Wang *et al.*, Appl. Phys. Lett. **70**, 529 (1997).
[2] Y. Shibata *et al.*, Phys. Rev. E **52**, 6787 (1995).
[3] F. Zimmermann *et al.*, in *Proceedings of the 1997 Particle Accelerator Conference, Vancouver, Canada*, edited by M. Comyn *et al.* (IEEE, Piscataway, NJ, 1998), p. 2189.
[4] M. L. Ponds *et al.*, Nucl. Instrum. Methods Phys. Res., Sect. A **375**, 136 (1996).
[5] K. J. Woods *et al.*, Phys. Rev. Lett. **74**, 3808 (1995).
[6] M. Oyamada *et al.*, in *Proceedings of the 1993 Particle Accelerator Conference, Washington, DC*, edited by S. T. Corneliussen (IEEE, New York, 1993), p. 1614.
[7] D. Oepts *et al.*, in *Proceedings of the Twenty-First International Free Electron Laser Conference, Hamburg, 1999* (Elsevier, Amsterdam, 2000).
[8] C. W. Rella *et al.*, Opt. Commun. **157**, 335 (1998).
[9] Todd Smith, in *Proceedings of the Twenty-First International Free Electron Laser Conference, Hamburg, 1999* (Ref. [7]).
[10] R. Lai, U. Happek, and A. J. Sievers, Phys. Rev. E **50**, R4294 (1994).
[11] M. Uesaka *et al.*, Nucl. Instrum. Methods Phys. Res., Sect. A **406**, 371 (1998).
[12] D. X. Wang, G. A. Krafft, and C. K. Sinclair, Phys Rev E **57**, 2283 (1998).
[13] E. R. Crosson *et al.*, in *Micro Bunches Workshop*, edited by M. Blum *et al.*, AIP Conf. Proc. No. 367 (AIP, New York, 1996), p. 397.
[14] K. N. Ricci, E. R. Crosson, and T. I. Smith, Nucl. Instrum. Methods Phys. Res., Sect. A (to be published).
[15] Gi. Schneider *et al.*, Nucl. Instrum. Methods Phys. Res., Sect. A **396**, 283 (1997).
[16] J. D. Jackson, *Classical Electrodynamics* (Wiley and Sons, New York, 1975), 2nd ed., p. 438.
[17] H. Wiedemann *et al.*, J. Nucl. Mater. **248**, 374 (1997).
[18] K. L. Brown, SLAC Report No. 75, 1982.
[19] David Carey, *The Optics of Charged Particle Beams* (Harwood Academic Publishers, Chur, Switzerland, 1987), p. 125.
[20] W. B. Colson, in *Laser Handbook: Free Electron Lasers*, edited by W. B. Colson, C. Pellegrini, and A. Renieri (Elsevier, Amsterdam, 1990), Vol. 6, pp. 118,136.
[21] N. Piovella *et al.*, Phys. Rev. E **52**, 5470 (1995).
[22] A. Tremaine *et al.*, Phys. Rev. Lett. **81**, 5816 (1998).